Water Research 182 (2020) 115921

Contents lists available at ScienceDirect

Water Research

journal homepage: www.elsevier.com/locate/watres

Degradation and deactivation of a plasmid-encoded extracellular antibiotic resistance gene during separate and combined exposures to UV_{254} and radicals

Maolida Nihemaiti [a, 1], Younggun Yoon [b, 1], Huan He [c], Michael C. Dodd [c], Jean-Philippe Croué [a, d, **], Yunho Lee [b, *]

[a] Curtin Water Quality Research Centre, Department of Chemistry, Curtin University, GPO Box U1987, Perth, 6845, Australia
[b] School of Earth Sciences and Environmental Engineering, Gwangju Institute of Science and Technology (GIST), Gwangju, 61005, Republic of Korea
[c] Department of Civil and Environmental Engineering, University of Washington, Seattle, WA, 98195-2700, United States
[d] Institut de Chimie des Milieux et des Materiaux IC2MP UMR 7285 CNRS, Universite de Poitiers, France

ARTICLE INFO

Article history:
Received 23 January 2020
Received in revised form
17 April 2020
Accepted 5 May 2020
Available online 16 May 2020

Keywords:
Antibiotic resistant bacteria
Antibiotic resistance genes
Gene transformation
UV
Hydroxyl radical
Sulfate radical

ABSTRACT

This study investigated the degradation and deactivation of an extracellular ampicillin resistance gene (amp^R) encoded in plasmid pUC19 during exposure to UV_{254}, $^{\bullet}OH$ (generated by $UV_{>290}/H_2O_2$), and combined exposure to UV_{254} and $^{\bullet}OH$ (and/or $SO_4^{\bullet-}$) using UV_{254}/H_2O_2 and $UV_{254}/S_2O_8^{2-}$. The degradation rates of amp^R measured by quantitative polymerase chain reaction increased with increasing target amplicon length (192–851 bps). The rate constants for the degradation of pUC19 (2686 bps) were calculated as 0.26 cm^2/mJ for UV_{254} and 1.5×10^{11} $M^{-1}s^{-1}$ for $^{\bullet}OH$, based on the degradation rates of amp^R amplicons and assuming an equal sensitivity of DNA damage across the entire plasmid. DNA repair-proficient *Escherichia coli (E. coli)* AB1157 strain (wild-type) and its repair-deficient mutants including AB1886 (*uvrA*$^-$), AB2463 (*recA*$^-$), AB2480 (*uvrA*$^-$, *recA*$^-$), and DH5α (*recA*$^-$, *endA*$^-$) were applied as recipient cells in gene transformation assays. Results suggested that the elimination efficiency of transforming activity during UV_{254} and $^{\bullet}OH$ exposure was dependent on the type of DNA repair genes in recipient *E. coli* strains. Losses of transforming activity were slower than the degradation of pUC19 by a factor of up to ~5 (for *E. coli* DH5α), highlighting the importance of DNA repair in recipient cells. The degradation rates of amp^R amplicons were much larger (by a factor of ~4) in UV_{254}/H_2O_2 and $UV_{254}/S_2O_8^{2-}$ than UV_{254} direct photolysis, indicating the significant contribution of $^{\bullet}OH$ and $SO_4^{\bullet-}$ to the gene degradation. Not only UV_{254} and $SO_4^{\bullet-}$, but also $^{\bullet}OH$ contributed to the degradation of amp^R during $UV_{254}/S_2O_8^{2-}$, which was attributed to the conversion of $SO_4^{\bullet-}$ to $^{\bullet}OH$ and a 10-fold larger reactivity of $^{\bullet}OH$ towards amp^R as compared to $SO_4^{\bullet-}$. However, the enhanced gene degradation by radicals did not lead to a faster elimination of gene transforming activity during UV_{254}/H_2O_2 and $UV_{254}/S_2O_8^{2-}$, suggesting that UV_{254}- and radical-induced DNA damage were not additive in their contributions to losses of gene transforming activity. Wastewater effluent organic matter (EfOM) accelerated the degradation of amp^R during UV_{254} irradiation by means of reactive species production through indirect photolysis reactions, whereas EfOM mainly acted as a radical scavenger during UV_{254}/H_2O_2 and $UV_{254}/S_2O_8^{2-}$ treatments.

Abbreviations: amp^R, Ampicillin Resistance Gene; AOPs, Advanced Oxidation Processes; Amp, Amplicon; ARB, Antibiotic Resistant Bacteria; ARG(s), Antibiotic Resistance Gene(s); bp(s), Nucleotide Base Pair(s); DOM, Dissolved Organic Matter; e-ARG, Extracellular Antibiotic Resistance Genes; *E. coli*, *Escherichia coli*; EfOM, Effluent Organic Matter; *p*CBA, *para*-Chlorobenzoic Acid; qPCR, Quantitative Polymerase Chain Reaction.

* Corresponding author. School of Earth Sciences and Environmental Engineering, Gwangju Institute of Science and Technology (GIST), Gwangju 61005, Republic of Korea.
** Corresponding author. Curtin Water Quality Research Centre, Department of Chemistry, Curtin University, GPO Box U1987, Perth, 6845, Australia.
E-mail addresses: jean.philippe.croue@univ-poitiers.fr (J.-P. Croué), yhlee42@gist.ac.kr (Y. Lee).
[1] M. Nihemaiti and Y. Yoon contributed equally to this work.

https://doi.org/10.1016/j.watres.2020.115921
0043-1354/

1. Introduction

Antibiotic resistance is a natural phenomenon. However, anthropogenic activities (e.g., overuse and disposal of antibiotics) are providing constant selection pressure on antibiotic resistant bacteria (ARB) (Vikesland et al., 2017). Antibiotic resistance can be developed and disseminated within the bacterial population by genetic mutation, cell division, and the transfer of antibiotic resistance genes (ARGs) (Davies and Davies, 2010). ARGs are contaminants of concern in natural and engineered aquatic systems, as ARG transfer can be linked with the spread of antibiotic resistance to human pathogens (Dodd, 2012; Pruden, 2014). Mobile genetic elements carrying ARGs (e.g., plasmids, integrons, and transposons) can be disseminated to and expressed by recipient cells through horizontal gene transfer (HGT), including conjugation (mediated by cell to cell contact), transduction (bacteriophage mediated), and transformation (mediated by extracellular DNA) (Lorenz and Wackernagel, 1994). Of these, transformation can be understood to represent the most basic mode of HGT, as it does not require the presence of live donor cells or bacteriophages (Lorenz and Wackernagel, 1994). Consequently, quantification of the frequency with which an ARG in extracellular DNA can be transported into and expressed by a recipient cell through transformation (hereafter referred to as *transforming activity*) can provide a conservative measure of the ability of an ARG to undergo HGT. Transforming activity encompasses (a) efficiency of extracellular DNA transport into a recipient cell, (b) any repair of that DNA by the recipient cell in the event that the DNA is damaged, and (c) heritable incorporation and expression of the DNA's genetic information by recipient cells, and is therefore a function of both the recipient cell's ability to import, repair, and express a given ARG and the quality and quantity of the extracellular DNA containing the ARG. Extracellular DNA can be released into the environment though secretion by live cells and lysis of dead cells. While unstable to nucleases likely to be present in many aquatic matrixes, it can persist in the environment through adsorption onto soil and sediments (Lorenz and Wackernagel, 1994; Mao et al., 2014; Nagler et al., 2018).

Although conventional disinfection processes during water treatment (e.g., chlorine and UV) efficiently inactivate ARB, intracellular ARGs are more difficult to degrade (McKinney and Pruden, 2012; Yoon et al., 2017; He et al., 2019) and can be released into water following the death of ARB cells (Zheng et al., 2017). Sub-inhibitory concentrations of disinfectants (e.g., chlorine and monochloramine) were even reported to promote the horizontal transfer of ARGs by increasing the permeability of cell membranes and altering the expression of conjugation-related genes (Guo et al., 2015; Zhang et al., 2017). The proportion of extracellular DNA carrying ARGs was found to increase after various biological and chemical processes in wastewater treatment, revealing the potential risk of antibiotic resistance dissemination in discharged effluent and receiving environments (Liu et al., 2018; Zhang et al., 2018). Previous studies have reported the enrichment of ARGs in surface water due to the discharged effluents from upstream wastewater treatment plants (Cacace et al., 2019; Wu et al., 2019; Osińska et al., 2020). High diversity of ARGs in reclaimed wastewater (e.g., agriculture irrigation, potable reuse) may pose risks of antibiotic resistance dissemination to environmental bacteria and even human pathogens (Christou et al., 2017; Hong et al., 2018).

UV-based advanced oxidation processes (UV-AOPs) are increasingly applied for the removal of refractory contaminants during water treatment. The elimination of contaminants in UV-AOP treatment is achieved by dual pathways, namely direct UV photolysis (depending on the UV absorbances and quantum yields of target compounds) and oxidation by powerful radical species (Stefan, 2018). The activation of hydrogen peroxide (UV/H_2O_2) and peroxydisulfate ($UV/S_2O_8^{2-}$) by UV light produces hydroxyl radical ($^{\bullet}OH$) and sulfate radical ($SO_4^{\bullet-}$), respectively, which can degrade a wide range of contaminants, as these two radicals react with many compounds at or near diffusion-controlled reaction rates (Buxton et al., 1988; Neta et al., 1988).

UV/H_2O_2 and $UV/S_2O_8^{2-}$ have also been reported to efficiently inactivate ARB cells (Michael-Kordatou et al., 2015; Ferro et al., 2016; Giannakis et al., 2018). However, detailed investigation into the reactivity of $^{\bullet}OH$ with intracellular ARGs in these studies was limited due to the significant consumption of $^{\bullet}OH$ by constituents of the water matrix and cell membranes before reaching the cell interiors (Ferro et al., 2017; Yoon et al., 2017; Zhang et al., 2019a). Recent studies have reported that the reactivity of $^{\bullet}OH$ with extracellular chromosomal ARGs is highly dependent on the length of the monitored ARG targets (He et al., 2019). More studies are needed to assess whether the observed reactivities are generally applicable to other types of DNA such as plasmid-encoded ARGs. To the best of the authors' knowledge, little is known on the fate of ARGs during $SO_4^{\bullet-}$-based treatment processes.

Quantitative polymerase chain reaction (qPCR) has been widely applied to quantify structurally-intact ARGs or to measure their degradation rates in water and wastewater treatment (McKinney and Pruden, 2012; Luby et al., 2016; Hiller et al., 2019). It should be noted that qPCR methods usually record the degradation of a small fraction of a target ARG's sequence length (with amplicon sizes typically <1000 bps), and not the entirety of a gene (McKinney and Pruden, 2012; Chang et al., 2017; Yoon et al., 2018). In addition, the efficiency of DNA replication (particularly of damaged DNA) in qPCR methods can be different from that observed in bacterial cells subjected to transformation with the same DNA. Furthermore, the uptake and repair of DNA by recipient cells can play important roles in modulating gene transforming activity (Chang et al., 2017; Yoon et al., 2018). While the correlation between the degradation of target ARG amplicons (measured by qPCR) and the elimination of ARG transforming activity was reasonably well explained for chromosomal ARGs (He et al., 2019), it is still less clear for plasmid-borne ARGs.

Exposure of DNA to UV and $^{\bullet}OH$ is known to induce different types of DNA damage (von Sonntag, 2006). UV-C generates cyclobutane-pyrimidine dimers (CPDs) as the predominant DNA lesions, while $^{\bullet}OH$ can induce DNA damage ranging from base oxidation to phosphate-sugar backbone breakages (Görner, 1994; Sinha and Häder, 2002; von Sonntag, 2006). It is currently not completely clear how the various type(s) of DNA damage resulting from UV, $^{\bullet}OH$, and $SO_4^{\bullet-}$ are related to the deactivation of ARGs; for example, whether DNA lesions such as CPDs (formed by direct UV irradiation) have the same effect on DNA transforming activity as phosphate-sugar backbone breakage by $^{\bullet}OH$ (generated by H_2O_2 or $S_2O_8^{2-}$ photolysis). Furthermore, in UV-AOPs, DNA lesions can be generated by both direct UV irradiation and radicals simultaneously.

The aim of this study was to investigate the fate of plasmid-encoded e-ARGs during the common UV at 254 nm water disinfection process (UV_{254}) and its related AOPs. Plasmid (pUC19) encoding an ampicillin resistance gene (amp^R) was purified from *Escherichia coli* (*E. coli*) host cells and exposed to UV_{254}, to UV_{254} in combination with $^{\bullet}OH$ or $SO_4^{\bullet-}$ (by using UV_{254}/H_2O_2 and $UV_{254}/S_2O_8^{2-}$), or to $^{\bullet}OH$ only (by combining UV at >290 nm with H_2O_2) (i.e., $UV_{>290}/H_2O_2$). $UV_{>290}/H_2O_2$ treatment was chosen to study the effect of $^{\bullet}OH$ only exposure because irradiation of H_2O_2 by $UV_{>290}$ can generate $^{\bullet}OH$, while neither $UV_{>290}$ irradiation nor H_2O_2 directly affect amp^R under these experimental conditions (detailed in Section 3.1). The treated plasmid samples were analysed by qPCR, gel electrophoresis, and ARG transformation assay. DNA repair-proficient *E. coli* AB1157 (wild-type), as well as repair-

deficient *E. coli* mutants including AB1886 (*uvrA*$^-$), AB2463 (*recA*$^-$), AB2480 (*uvrA*$^-$, *recA*$^-$), and DH5α (*recA*$^-$, *endA*$^-$) were employed as recipient cells in the ARG transformation assay. Competition kinetics methods using radical probe compounds were applied to measure the second-order rate constants of $^{\bullet}OH$ and $SO_4^{\bullet-}$ with *amp*^{R} segments. Experiments were also conducted in the presence of wastewater effluent organic matter (EfOM) to study the effect of dissolved organic matter (DOM) on the removal of e-ARGs.

2. Materials and methods

2.1. Chemical reagents

All chemicals were of analytical grade or higher and used as received without further purification. Ampicillin sodium salt (#A0166), agar powder (#A1296), sodium chloride (≥99.5%), *para*-chlorobenzoic acid (99%), and nitrobenzene (≥99%) were purchased from Sigma-Aldrich. Tryptone (#1612) and yeast extract (#1702) were supplied from Laboratorios CONDA. Hydrogen peroxide 30% (Thermo Fisher Scientific) and sodium peroxydisulfate (≥98%, Sigma-Aldrich) were used to prepare the stock solutions of H_2O_2 and $S_2O_8^{2-}$, respectively. All solutions were prepared in Milli-Q water (18 MΩ·cm, Millipore). EfOM was previously extracted from the discharged effluent of a wastewater treatment plant in Jeddah, Saudi-Arabia, with XAD resins (Zheng et al., 2014). Solutions of EfOM were prepared by dissolving the hydrophobic and transphilic fractions (2:1 by mass) of EfOM in phosphate buffer.

2.2. Plasmid preparation

Plasmid pUC19 was extracted from *E. coli* DH5α. pUC19 (2686 bp) is a commercially available *E. coli* vector carrying an ampicillin resistance gene (*amp*^{R}, 861 bp). One hundred μL of *E. coli* DH5α mid-exponential growth phase culture in LB broth medium with 50 mg/L of ampicillin was transferred into 150 mL of LB broth medium containing 50 mg/L of ampicillin and incubated overnight (200 rpm, 37 °C). Plasmids were extracted from this overnight stock solution using an AccuPrep Plasmid Mini Extraction kit (Bioneer, 2016). The concentration of recovered plasmid DNA was measured on a NanoDrop ND-2000 Spectrophotometer (NanoDrop Products, Wilmington, USA).

2.3. UV experiments

UV_{254}-based experiments were carried out with a UV quasi-collimated beam device equipped with a low-pressure mercury lamp emitting UV light primarily at 254 nm (Sankyo Denki Ltd., Tokyo, Japan). The UV light was collimated onto the experimental solution, which was contained in a petri dish placed on a magnetic stirrer. The average UV intensity (0.3 mW/cm^2) was determined with atrazine chemical actinometry (Lee et al., 2016). Experimental solutions were prepared in autoclaved 2 mM phosphate buffer at pH 7. The initial concentration of plasmid DNA used in experiments was 0.3 or 1 μg/mL. The applied UV fluences ranged from 0 to 180 mJ/cm^2. The initial concentrations of H_2O_2 and $S_2O_8^{2-}$ were 0.5 mM for UV_{254}/H_2O_2 and $UV_{254}/S_2O_8^{2-}$, respectively. $UV_{>290}/H_2O_2$ experiments were conducted using a Model 66924 arc lamp source fitted with a 450-W O_3-free Xe arc lamp and focusing collimator, and equipped with an atmospheric attenuation filter and dichroic mirror to restrict lamp output to near-UV wavelengths ($290\ nm < \lambda < 400\ nm$) (Newport-Oriel Model 66924; Stratford, CT). Relatively high H_2O_2 concentrations (i.e., 10 mM) were applied for $UV_{>290}/H_2O_2$, in order to increase the yield of $^{\bullet}OH$ due to the low absorbance of UV light by H_2O_2 in this wavelength region. Samples were withdrawn from the irradiated solutions in each experimental setup at predetermined time intervals for DNA and probe compound analyses. Residual H_2O_2 and $S_2O_8^{2-}$ were quenched with bovine catalase and thiosulfate, respectively. Samples for DNA analysis (500 μL) were stored at −20 °C and analysed within 24 h. Control experiments indicated that H_2O_2 and $S_2O_8^{2-}$ did not affect qPCR analyses within these experimental conditions (Fig. S1).

2.4. Radical probe compounds

para-chlorobenzoic acid (*p*CBA) was used as $^{\bullet}OH$ probe during UV_{254}/H_2O_2 and $UV_{>290}/H_2O_2$ experiments. Both *p*CBA and nitrobenzene were applied during $UV_{254}/S_2O_8^{2-}$. Nitrobenzene can be used as a selective $^{\bullet}OH$ probe compound ($k_{\bullet OH}=3.9\times10^9\ M^{-1}\ s^{-1}$) (Buxton et al., 1988) due to its low reactivity to $SO_4^{\bullet-}$ ($k_{SO_4^{\bullet-}}<10^6\ M^{-1}\ s^{-1}$) (Neta et al., 1977), whereas *p*CBA reacts with both radicals (i.e., $k_{SO_4^{\bullet-}} = 3.6\times10^8\ M^{-1}\ s^{-1}$ and $k_{\bullet OH}=5\times10^9\ M^{-1}\ s^{-1}$) (Neta et al., 1977; Buxton et al., 1988). *p*CBA and nitrobenzene were analysed on a high-performance liquid chromatograph (HPLC, Dionex Ultimate 3000, Thermo Scientific) equipped with an XDB-C18 column (5 μm, 4.6 × 150 mm, Agilent). The mobile phase comprised acetonitrile and 10 mM phosphoric acid (40:60, v/v). The two probe compounds were analysed at their maximum absorbance wavelengths (i.e., 240 and 270 nm for *p*CBA and nitrobenzene, respectively).

2.5. qPCR analysis

Gene degradation was measured by qPCR using a CFX96 real-time PCR detection system (Bio-Rad, Hercules, CA, USA). Four different amplicons (i.e., 192, 400, 603, and 851 bp) were monitored, which covered varying fractions of *amp*^{R} as shown in Fig. S2. The longest size of *amp*^{R} segment targeted in qPCR was 851 bp instead of the whole *amp*^{R} gene (861 bp), due to the low amplification efficiency of the 861 bp amplicon in the qPCR method. The reaction mixture (20 μL) consisted of 1 μL of each primer, 1 μL of sample, 10 μL of EvaGreen® supermix, and 7 μL of autoclaved DNase free water. The qPCR protocol included one cycle at 95 °C for 2 min, 30 cycles at 95 °C for 5 s, an annealing step at 55 °C for 60 s, and an elongation at 72 °C for 20 s, followed by a melt curve analysis from 65 °C to 95 °C. Each sample was analysed in triplicate. More information on qPCR analysis, the DNA sequence of *amp*^{R}, and the monitored qPCR target amplicons is described elsewhere (Yoon et al., 2018).

2.6. Gel electrophoresis analysis

pUC19 plasmid (1 μg/mL) treated by UV_{254} and $^{\bullet}OH$ ($UV_{>290}/H_2O_2$) was analysed by gel electrophoresis to investigate the structural change of plasmid DNA. Linearized pUC19 was also prepared for use as a reference by incubating the plasmid with type II restriction enzyme *EcoRI* (NEB, USA) at 37 °C for 1 h, followed by enzyme inactivation at 65 °C for 20 min. Plasmid samples from UV_{254}, $^{\bullet}OH$ ($UV_{>290}/H_2O_2$), and enzyme treatments, as well as a 1 kb DNA ladder (Enzynomics, Korea) were loaded on 0.8% agarose gels at 4 V cm^{-1} for 35 min. The bands were visualized by ethidium bromide staining. Gel images were captured on a UV trans-illuminator (Universal mutation detection system, UVP, LLC, USA).

2.7. Gene transformation assays

Non-ampicillin resistant *E.coli* K12 bacteria strains DH5α (*recA*$^-$, *endA*$^-$), AB1157 (wild-type), AB1886 (*uvrA*$^-$), AB2463 (*recA*$^-$), and AB2480 (*uvrA*$^-$, *recA*$^-$) were used as recipient cells for gene transformation assays. DH5α strain was commercially available from

ATCC; other strains were provided by CGSC (Coli Genetic Stock Center at Yale University). Details on transformation assays were described by Yoon et al. (2018). In brief, competent cells were prepared by chemical treatment of non-resistant *E. coli* K12 strains using calcium chloride and glycerol (Shanehbandi et al., 2013) and preserved at −80 °C until use. Fifty μL of treated plasmid sample was mixed with 100 μL of thawed competent cells. After incubating in ice for 30 min, the mixture was quickly transferred onto a digital test tube heater (45 °C) for 45 s and then placed back in ice for 2 min. After the heat shock, the samples were mixed with 900 μL of LB broth and cultured for 45 min (200 rpm, 37 °C). Finally, the incubated samples were serially diluted with LB broth and plated onto two types of LB agar plates (i.e., with and without inclusion of 50 mg/L of ampicillin). After 24 h of incubation at 37 °C, the number of ARB colonies (transformants) detected on selective agar plates (with ampicillin) were compared with the total recipient cells growing on nonselective agar plates (without ampicillin). The gene transformation efficiency was calculated as follows:

$$\text{Transformation efficiency} = \frac{Transformant\ cells_{selective\ plate}(CFU/mL)}{Total\ recipient\ cells_{nonselective\ plate}\ (CFU/mL)}$$

The typical concentrations of total recipient cells, as measured by culturing on nonselective agar plates (without ampicillin), were approximately 3×10^8 and 2×10^8 CFU/mL for *E. coli* DH5α and *E. coli* AB strains, respectively. Control experiments conducted by directly plating the recipient cells (without heat shock) on nonselective plates showed <10% variation in the final colony counts of recipient cells as compared to the conditions incorporating heat shock (Fig. S3), and <50% variation in colony counts between strains. These results indicated that the type of bacterial strain used, or stresses to which the strains were subjected during transformation assays (e.g., heat shock), did not significantly impact the fitness or growth rates of recipient cells on nonselective plates. Calibration curves prepared with known concentrations of plasmid DNA indicated that the number of transformants linearly increased with increasing plasmid DNA concentration from 10^{-5}–10^{-1} μg/mL (Fig. S4). The transformation efficiency of amp^R calculated for *E. coli* K12 strains was in the range of $10^{-4} - 10^{-8}$, which was comparable with previous studies (Chang et al., 2017; Yoon et al., 2018).

2.8. Statistical analysis

Statistical analysis was conducted using SigmaPlot 12.0 and GraphPad Prism 7.0. The fluence-based rate constants for gene degradation and transformation efficiency loss under various experimental conditions were obtained by linear regression analysis and compared by performing the Analysis of Covariance (ANCOVA). The null hypothesis was that the first-order rate constants were identical, with $p = 0.05$ as the threshold significance level.

3. Results and discussions

3.1. e-ARG degradation during separate exposure to UV_{254} and $^{\bullet}OH$

UV_{254} exposure (Fig. 1a). The solution containing pUC19 was irradiated with UV_{254} light (0–130 mJ/cm^2). The degradation of amp^R segments (192, 400, 603, and 851 bp) measured by qPCR followed first-order kinetics with respect to UV fluence ($r^2 > 0.99$) (Fig. 1a). The 192 bp amp^R segment was degraded by about 1-log at 110 mJ/cm^2, whereas 4-log reduction was already achieved for the 851 bp segment, which was close to the overall size of amp^R (861 bp). The resulting fluence-based rate constants derived from the slopes of linear curves, $k_{UV,Amp} = 2.303 \times slope$, are summarized in Table 1. The $k_{UV,Amp}$ of amp^R segments increased with amplicon size, which was consistent with the increasing number of potential reaction sites with increasing number of nucleotide bps. The $k_{UV,Amp}$ values obtained from this study were comparable to previously-reported values for the same amp^R segments (Yoon et al., 2018). The $k_{UV,plasmid}$ of pUC19 plasmid could be estimated by extrapolating the $k_{UV,Amp}$ of each segment to the entire plasmid (e.g., $k_{UV,plasmid} = k_{UV,192bp} \times \frac{2686\ bp}{192\ bp}$), based on an assumption that the UV reactivity per base pair is the same across the entire plasmid. The $k_{UV,plasmid}$ values estimated from the 192, 400, 603, and 851 bp amplicons were $2.9(\pm0.06) \times 10^{-1}$, $2.3(\pm0.04) \times 10^{-1}$, $2.6(\pm0.05) \times 10^{-1}$, and $2.7(\pm0.06) \times 10^{-1}$ cm^2/mJ, respectively, yielding an average $k_{UV,plasmid}$ value of $2.6(\pm0.05) \times 10^{-1}$ cm^2/mJ (Table 1).

A theoretical approach was recently employed to estimate the photoreactivity of DNA (i.e., formation rate of CPDs and 6,4-photoproducts) based on the molar absorption coefficients, quantum yields, and the number of 5′-bipyrimidine-3′ doublets of a given DNA (Yoon et al., 2018; He et al., 2019). By applying this approach, the theoretical overall DNA lesion formation rate on pUC19 upon UV_{254} exposure, $k_{all\ lesions}$, was calculated as 2.1×10^{-1} cm^2/mJ (Text S1), which was close to the average $k_{UV,plasmid}$ (2.6×10^{-1} cm^2/mJ) determined from qPCR results as mentioned above.

$^{\bullet}OH$ exposure (Fig. 1b). Control experiments have confirmed that amp^R segments were stable under $UV_{>290}$ irradiation alone (Fig. S5), which was attributed to the low UV absorbance of plasmid DNA above 290 nm. Moreover, 10 mM (340 mg/L) of H_2O_2 had negligible effect on the amp^R segment (Fig. S1). Thus, $UV_{>290}/H_2O_2$ was applied to investigate the influence of $^{\bullet}$OH on the degradation of e-ARG. The $^{\bullet}$OH exposure, $\int[\bullet OH]dt$, in the $UV_{>290}/H_2O_2$ system was obtained by following the degradation of *p*CBA, which was additionally included in the experimental solution. No $UV_{>290}$ direct photolysis of *p*CBA was observed in the absence of H_2O_2 (Fig. S6). Thus, the $^{\bullet}$OH exposure was calculated from $\int[^{\bullet}OH]dt = -\frac{ln\frac{[pCBA]}{[pCBA]_0}}{k_{\bullet OH,pCBA}}$ (Elovitz and von Gunten, 1999), where $k_{\bullet OH,pCBA}$ is the second-order rate constant of $^{\bullet}$OH with *p*CBA (5×10^9 M^{-1} s^{-1}) (Buxton et al., 1988). The logarithmic-scale degradation of amp^R segments exhibited linear correlations with $^{\bullet}$OH exposure during $UV_{>290}/H_2O_2$ (Fig. 1b). The resulting bimolecular rate constants derived from the slopes of linear curves, $k_{\bullet OH,Amp} = 2.303 \times slope$, are summarized in Table 1.

The $k_{\bullet OH,Amp}$ of amp^R segments increased with amplicon size, ranging from 8.1×10^9 M^{-1} s^{-1} for the 192 bp amplicon to 5.6×10^{10} M^{-1} s^{-1} for the 851 bp amplicon (Table 1). A good linear relationship ($r^2 = 0.996$) was observed between the $k_{\bullet OH,Amp}$ and the base pair number of amp^R segments (Fig. S7), which was consistent with previous findings that $^{\bullet}$OH non-selectively reacts with all nucleotides in a DNA sequence (both AT and GC contents)

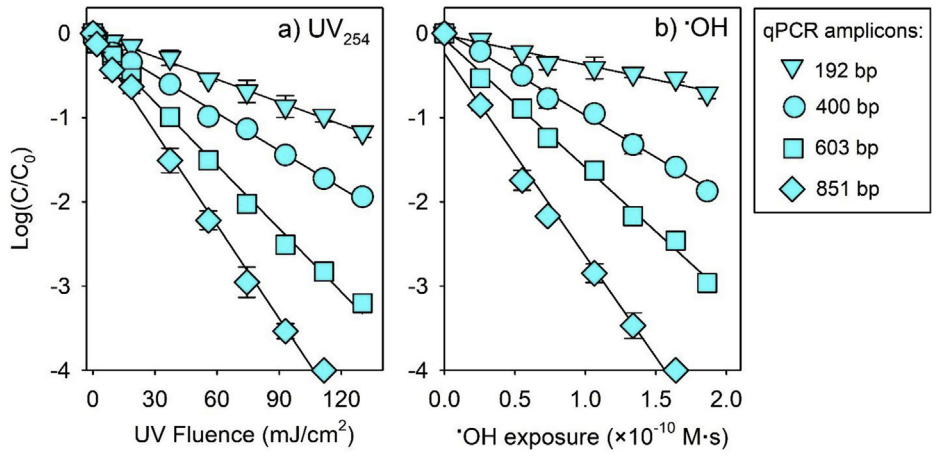

Fig. 1. Degradation of amp^R segments during the treatment of pUC19 (1 μg/mL) with (a) UV_{254} and (b) •OH ($UV_{>290}/H_2O_2$) at pH 7 (2 mM phosphate buffer). 10 mM of H_2O_2 and 1 μM of *p*CBA were added in $UV_{>290}/H_2O_2$ experiments. Error bars represent the standard deviations of triplicate experiments. Lines are the linear regressions of the experimental data.

Table 1
Apparent rate constants for the degradation of amp^R segments and pUC19 plasmid, and the elimination of gene transforming activity during UV_{254} and •OH only treatments[a].

amp^R segments		pUC19 plasmid[b]		Loss of gene transformation	
#base pairs (bps)	k_{Amp}	$k_{plasmid}$	average	Recipient cells	$k_{transformation}$
		UV_{254} (cm^2/mJ)			
192	$2.0(\pm0.05) \times 10^{-2}$	$2.9(\pm0.06) \times 10^{-1}$	$2.6(\pm0.05) \times 10^{-1}$	DH5α	$6.5(\pm0.21) \times 10^{-2}$
400	$3.4(\pm0.07) \times 10^{-2}$	$2.3(\pm0.04) \times 10^{-1}$		AB1157	$1.0(\pm0.03) \times 10^{-1}$
603	$5.8(\pm0.11) \times 10^{-2}$	$2.6(\pm0.05) \times 10^{-1}$		AB1886	$2.4(\pm0.06) \times 10^{-1}$
851	$8.9(\pm0.16) \times 10^{-2}$	$2.7(\pm0.06) \times 10^{-1}$		AB2463	$1.6(\pm0.06) \times 10^{-1}$
		•OH ($UV_{>290}/H_2O_2$) (M^{-1} s^{-1})			
192	$8.1(\pm0.69) \times 10^{9}$	$1.2(\pm0.10) \times 10^{11}$	$1.5(\pm0.07) \times 10^{11}$	DH5α	$2.7(\pm0.05) \times 10^{10}$
400	$2.2(\pm0.07) \times 10^{10}$	$1.5(\pm0.05) \times 10^{11}$		AB1157	$4.1(\pm0.14) \times 10^{10}$
603	$3.5(\pm0.10) \times 10^{10}$	$1.6(\pm0.04) \times 10^{11}$		AB1886	$6.5(\pm0.18) \times 10^{10}$
851	$5.6(\pm0.27) \times 10^{10}$	$1.8(\pm0.08) \times 10^{11}$		AB2463	$8.2(\pm0.23) \times 10^{10}$

[a] Experimental conditions: pUC19: 1 μg/mL, 2 mM phosphate buffer at pH 7, fluence range for UV_{254}: 0–130 mJ/cm^2, 10 mM of H_2O_2 and 1 μM of *p*CBA were added in $UV_{>290}/H_2O_2$. The apparent rate constant values were reported in the form of Mean ± Standard Error.
[b] The $k_{plasmid}$ values of pUC19 plasmid were estimated based on the k_{Amp} of amp^R segments obtained from qPCR analyses (see Section 3.1 for details).

(He et al., 2019). The $k_{\bullet OH,plasmid}$ of the entire plasmid was predicted to be 1.8×10^{11} M^{-1} s^{-1} by applying the base pair number of pUC19 (2686 bps) into the regression equation of this linear relationship (Fig. S7). Alternatively, similar to $k_{UV,plasmid}$ as mentioned above, the $k_{\bullet OH,plasmid}$ of pUC19 was also estimated by normalizing the $k_{\bullet OH,\ Amp}$ of each segment (qPCR analyses) to the entire plasmid and calculating the average value as $1.5(\pm0.07) \times 10^{11}$ M^{-1} s^{-1} (Table 1).

The $k_{\bullet OH,Amp}$ values for the plasmid-encoded amp^R segments in this study were lower by a factor of ~3 than those reported for the chromosome-encoded *blt* genes with similar amplicon length (He et al., 2019). To see whether the reactivity difference is due to the conformational difference between the supercoiled-form plasmid and linear-form genomic DNA, the theoretical diffusion-controlled rate constant for the reaction of •OH with supercoiled pUC19 was calculated based on a method proposed by He et al. (2019). The theoretical maximum $k_{\bullet OH}$ value was predicted as 3.84×10^{11} M^{-1} s^{-1} for pUC19, which yields a bp-specific $k_{\bullet OH}$ value of 1.43×10^{8} M_{AT+GC}^{-1} s^{-1} when normalized to the length (in AT + GC bps) of pUC19 (2686 bps) (Text S2). For comparison, the theoretical maximum $k_{\bullet OH}$ value was 7.97×10^{12} M^{-1} s^{-1} for a hypothetical 50-kbp linear-form segment of genomic DNA, yielding a bp-specific $k_{\bullet OH}$ value of 1.59×10^{8} M_{AT+GC}^{-1} s^{-1} (He et al., 2019). This indicates that the conformational difference between the plasmid (supercoiled) and genomic (linear) DNA (the bp-specific $k_{\bullet OH}$ differed only by a factor of 1.1) does not explain the observed •OH reactivity difference. The maximum $k_{\bullet OH}$ values for the amp^R amplicons can also be calculated by multiplying the bp-specific $k_{\bullet OH}$ (1.43×10^{8} M_{AT+GC}^{-1} s^{-1}) with the length of each amplicon, and ranged from 2.57×10^{10} M^{-1} s^{-1} for 192 bp to 1.14×10^{11} M^{-1} s^{-1} for 851 bp (Text S2). Thus, the experimental $k_{\bullet OH,\ Amp}$ for pUC19 were lower by a factor of 2.5 than the theoretical maximum $k_{\bullet OH,\ Amp}$ values. This difference is acceptable considering all possible experimental errors as well as uncertainties of parameters used in the model applied in the theoretical calculation.

Structural degradation of plasmid (Fig. 2). Fig. 2a shows the electrophoresis gel of pUC19 exposed to UV_{254}. The intact pUC19 before the UV_{254} exposure showed a band located lower than the pUC19 linearized by *EcoRI*. Plasmid DNA generally exists in a supercoiled form, which is smaller than its linear form and migrates faster in electrophoresis gel. The UV_{254} irradiation (0–130 mJ/cm^2) did not change the position of the band, suggesting that the pUC19 kept its supercoiled form without significant conformational change (e.g., strand breakage). It is well documented that the gene damage by UV_{254} is mainly caused by the formation of DNA lesions such as CPDs and 6,4-photoproducts (pyrimidine adducts) (Sinha and Häder, 2002; Cadet and Douki, 2018), which are generally not detectable by gel electrophoresis analysis (Yoon et al., 2018).

The reaction pathways of •OH with DNA include addition to nucleobases – producing adduct radicals – and hydrogen-abstraction from 2-deoxyribose (sugar moiety) (von Sonntag, 2006; Dizdaroglu and Jaruga, 2012), resulting in not only oxidized

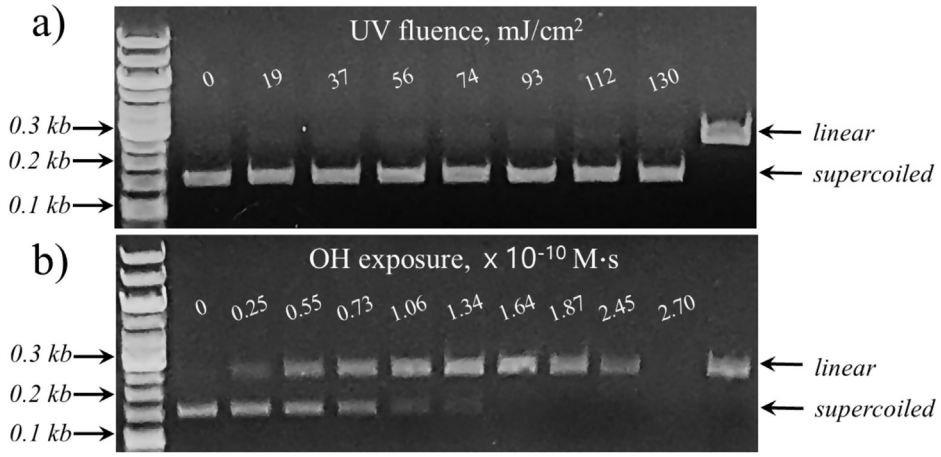

Fig. 2. DNA electrophoresis gel of pUC19 treated by (a) UV_{254} and (b) $^{\bullet}OH$ ($UV_{>290}/H_2O_2$). First column shows the standard DNA ladders. Last column shows the linearized pUC19 after treating with *EcoRI* restriction digestion.

bases and abasic sites, but also strand breaks (Cadet et al., 1999; von Sonntag, 2006). The double-strand breaks are expected to be mainly responsible for the conformational change from supercoiled to linear plasmid form. Gel electrophoresis analysis showed that the pUC19 plasmid band gradually moved from the supercoiled to linear form position with increasing $^{\bullet}OH$ exposure (Fig. 2b), revealing the formation of double-strand breaks in pUC19.

3.2. e-ARG deactivation (loss of transforming activity) during separate exposure to UV_{254} and $^{\bullet}OH$

Bacterial cells have developed the ability of repairing DNA lesions induced by UV irradiation and oxidant stress (e.g., radicals) using several enzyme systems (Teebor et al., 1988; Sinha and Häder, 2002). The biological deactivation of pUC19 upon separate treatment with UV_{254} and $^{\bullet}OH$ was studied by analysing its transformation of non-resistant recipient cells having different DNA repair abilities. The decrease of transforming activity of pUC19 followed first-order kinetics with respect to UV fluence or $^{\bullet}OH$ exposure, and was variable depending on the recipient cells used (Fig. 3). The most rapid decrease was observed for AB2480 (*uvrA*$^-$, *recA*$^-$) during each separate treatment with UV_{254} and $^{\bullet}OH$. No transformant was detectable from AB2480 (more than 4-log decrease) when the UV fluence was above 5 mJ/cm^2, or when the $^{\bullet}OH$ exposure was higher than 5.5×10^{-11} M s. Thus, the fluence-based rate constant for UV ($k_{UV,transformation}$) and the second-order rate constant for $^{\bullet}OH$ ($k_{^{\bullet}OH,transformation}$) for the elimination of AB2480 transforming activity were not calculated in this case due to the limited data points.

During UV_{254} exposure (Fig. 3a), the loss of transforming activity was slower in AB1886 (*uvrA*$^-$, 0.24 cm^2/mJ) than AB2480, followed by AB2463 (*recA*$^-$, 0.16 cm^2/mJ), AB1157 (wild-type, 0.10 cm^2/mJ), and DH5α (*recA*$^-$, *endA*$^-$, 0.07 cm^2/mJ), where the values in parentheses show $k_{UV,\ transformation}$ (Table 1). The variation in the transformation efficiency of plasmids carrying the same DNA damage indicated that the UV-induced damage can be repaired by recipient cells to different extents, depending on their repair gene proficiencies (or deficiencies). The *uvrABC* proteins involve the nucleotide excision repair of a variety of DNA lesions including the UV-induced CPDs and 6,4-photoproducts. This process is initiated by the interaction of *uvrA* protein with DNA to recognize the damaged sites (Kisker et al., 2013). The *recA* protein is essential for

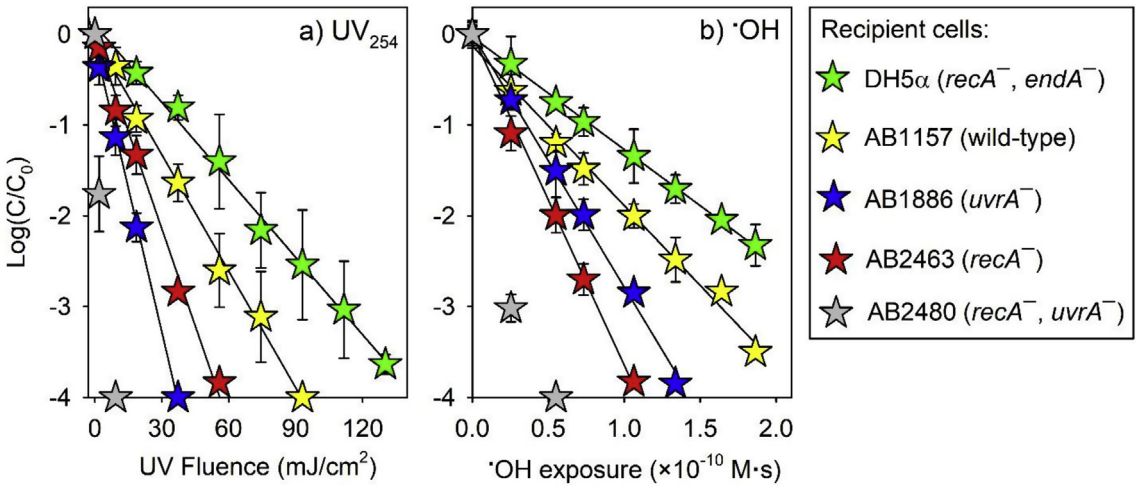

Fig. 3. Elimination of gene transforming activity during the treatment of pUC19 (1 μg/mL) with (a) UV_{254} and (b) $^{\bullet}OH$ ($UV_{>290}/H_2O_2$) at pH 7 (2 mM phosphate buffer). 10 mM of H_2O_2 and 1 μM of *p*CBA were added in $UV_{>290}/H_2O_2$ experiments. The parentheses in the legend show the deficient DNA repair genes in recipient cells. Error bars represent the standard deviations of triplicate experiments. Lines are the linear regressions of the experimental data.

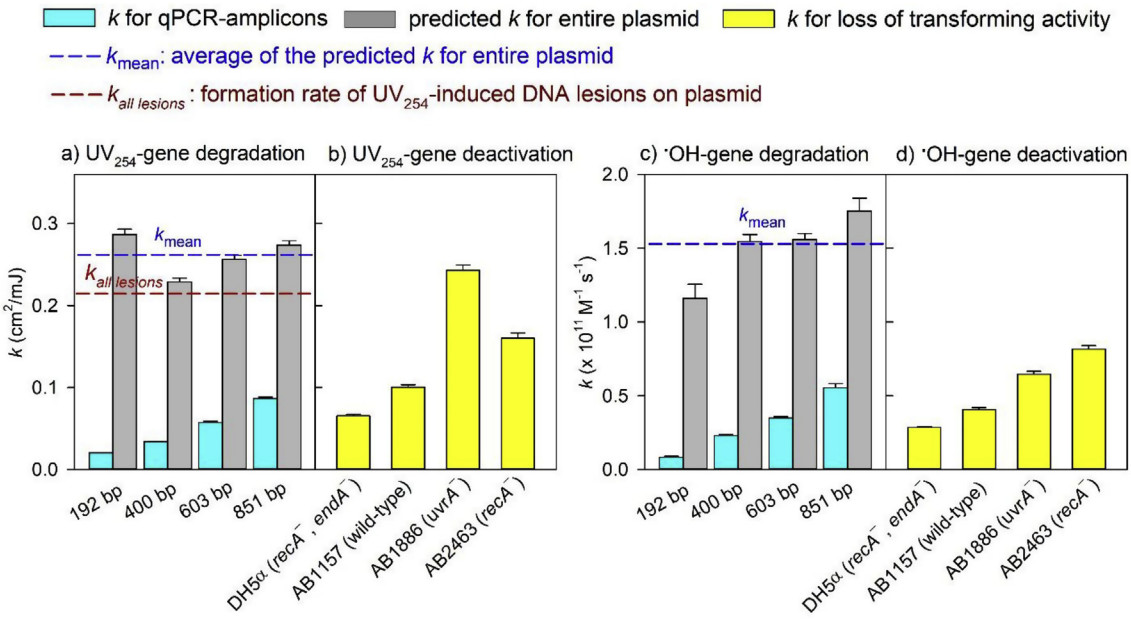

Fig. 4. Apparent rate constants for the degradation of amp^R segments, pUC19 plasmid, and the elimination of gene transforming activity during exposure to (a, b) UV_{254} and (c, d) $^{\bullet}OH$ ($UV_{>290}/H_2O_2$). Specific kinetic parameters are summarized in Table 1 and error bars represent the standard errors of apparent rate constants. Rate constants for the loss of transforming activity in AB2480 were not calculated due to the limited number of measurable data points obtained in experiments using AB2480 as a recipient strain.

the post-replication repair of double-strand breaks and single-strand gaps (e.g., T-T dimers) by homologous recombination (Smith and Wang, 1989; Shinohara and Ogawa, 1995). These roles of *uvrA and recA* proteins well explained the trend observed from the transformation rates of *E. coli* strains. AB2480 was most sensitive to UV-induced DNA damage on pUC19 due to lack of both *uvrA* and *recA* genes. The *uvrA* deficient AB1886 was the second most sensitive, followed by the *recA* deficient AB2463, indicating that *uvrA* played a more important role than *recA* for the repair of UV-induced DNA damage. The wild-type AB1157 was less sensitive than the other three *E. coli* mutant strains owing to its DNA repair capability by *uvrA* and *recA*. Interestingly, despite its deficiency in *recA*, the DH5α strain exhibited even lower sensitivity to UV-induced DNA damage compared to wild-type AB1157. This was possibly attributable to the lack of a functional *endA* gene in DH5α. The *endA* gene is associated with the formation of extracellular DNase I, which can hydrolyze exogenous plasmid DNA, consequently reducing its uptake and transformation (Shou et al., 2019). In line with this, the DH5α showed ~10-fold higher transformation efficiency than the other *E. coli* strains proficient in *endA* when all were transformed with equivalent concentrations of undamaged pUC19 (Fig. S4). This *endA* deficiency might therefore render *E. coli* DH5α inherently more active for DNA damage repair than the other strains, despite its lack of *recA*.

During $^{\bullet}OH$ exposure (Fig. 3b), the rate of transforming activity loss was the highest for AB2480 followed by AB2463 (*recA*$^-$, 8.2×10^{10} M^{-1} s^{-1}), AB1886 (*uvrA*$^-$, 6.5×10^{10} M^{-1} s^{-1}), AB1157 (wild-type, 4.1×10^{10} M^{-1} s^{-1}), and DH5α (*recA*$^-$, *endA*$^-$, 2.9×10^{10} M^{-1} s^{-1}), where the values in parentheses show $k_{^{\bullet}OH,\ transformation}$ (Table 1). The *recA* deficient AB2463 showed higher sensitivity to $^{\bullet}OH$-induced DNA damage than the *uvrA* deficient AB1886, which was opposite compared to the case for UV_{254} (Fig. 3a). This suggests that *recA* is more efficient for repairing $^{\bullet}OH$-induced DNA damage, as homologous recombination is based on exchange of (damaged) nucleotide sequences (Alberts et al., 2002) and capable of repairing not only base oxidation but also double-strand breaks. In contrast, *uvrA* is based on nucleotide excision repair and more specific to the repair of UV-induced DNA lesions (base modification such as CPDs), but not efficient for double-strand breaks (Alberts et al., 2002).

The apparent rate constants for the degradation of amp^R segments, pUC19 plasmid, and the loss of gene transforming activity are compared in Fig. 4. For both UV_{254} direct photolysis and $^{\bullet}OH$ oxidation, the estimated degradation rates of the entire plasmid (based on qPCR analyses) overestimated the rates of pUC19 deactivation (loss of transforming activity) observed for all repair-proficient *E. coli* recipient strains, which can be explained by the repair of UV_{254}- and $^{\bullet}OH$-induced damage by repair-proficient recipient cells. Our results were in agreement with previous findings on the UV_{254} treated pWH1266 plasmid and its transformation of *Acinetobacter baylyi* (Chang et al., 2017). However, the rate of gene deactivation during UV_{254} direct photolysis measured using *uvrA* deficient AB1886 as the recipient strain was close to the estimated degradation rate of pUC19 and the formation rate of DNA lesions (Fig. 4a and b). The minimum rates of gene deactivation measured by double mutant AB2480 (*uvrA*$^-$, *recA*$^-$) were estimated based on the limited data points shown in Fig. 3, which gave 0.91 cm^2/mJ and 1.7×10^{11} M^{-1} s^{-1} for UV_{254} and $^{\bullet}OH$ exposure, respectively. These values were significantly larger than the gene deactivation rates measured by any of the repair proficient strains. Furthermore, the degradation rate of the entire plasmid underestimated the loss of pUC19 transforming activity measured by AB2480 (*uvrA*$^-$, *recA*$^-$) during UV_{254} direct photolysis and $^{\bullet}OH$ oxidation.

3.3. e-ARG degradation and deactivation by combined exposure to UV_{254} and radicals

The degradation of amp^R and the elimination of gene transforming activity (*E. coli* DH5α as recipient cells) were tested during combined exposure to UV_{254} and radicals ($^{\bullet}OH$ and $SO_4^{\bullet-}$), in comparison to UV_{254} direct photolysis. The degradation of amp^R amplicons followed first-order kinetics with respect to UV fluence ($r^2 > 0.99$) during UV_{254}, UV_{254}/H_2O_2, and $UV_{254}/S_2O_8^{2-}$ treatments

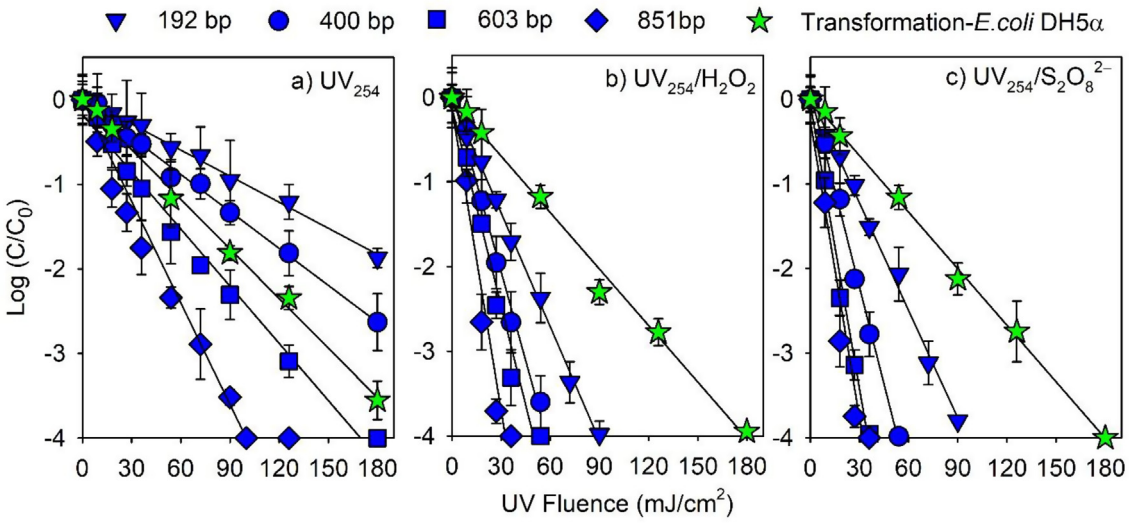

Fig. 5. Degradation of amp^R segments and elimination of gene transforming activity (*E.coli* DH5α as recipient cells) with increasing UV fluence (0–180 mJ/cm^2) during treatment of pUC19 (0.3 μg/mL) with (a) UV_{254}, (b) UV_{254}/H_2O_2 (0.5 mM), and (c) $UV_{254}/S_2O_8^{2-}$ (0.5 mM) at pH 7 (2 mM phosphate buffer). *p*CBA (1 μM) was added in UV_{254}/H_2O_2 experiments for the quantification of $^{\bullet}OH$, and both *p*CBA and nitrobenzene (each 1 μM) were added in $UV/S_2O_8^{2-}$ experiments for the quantification of $^{\bullet}OH$ and $SO_4^{\bullet-}$. Error bars represent the standard deviations of triplicate experiments. Lines represent the linear regressions of experimental data.

(Fig. 5). A lower initial concentration of pUC19 (0.3 μg/mL) and a higher fluence range (0–180 mJ/cm^2) were applied in these tests than in the experiments described in the preceding sections. However, the degradation rate constants of amp^R amplicons during UV_{254} direct photolysis (i.e., 2.4×10^{-2}–8.2×10^{-2} cm^2/mJ) (Table S1) were in good agreement with those obtained during the treatment of 1 μg/mL of pUC19 by 0–130 mJ/cm^2 of UV_{254} (i.e., 2.0×10^{-2}–8.9×10^{-2} cm^2/mJ, Table 1). The k_{UV_{254}/H_2O_2} of amp^R amplicons during UV_{254}/H_2O_2 were in the range of 1.0×10^{-1}–3.0×10^{-1} cm^2/mJ, which were larger than the $k_{UV_{254}}$ by a factor of ~4 (Table S1). Therefore, the contribution of UV_{254} direct photolysis to the overall gene degradation during UV_{254}/H_2O_2 was only about 25% ($k_{UV_{254}}/k_{UV_{254}/H_2O_2} \times 100\%$), revealing the significant role of $^{\bullet}OH$ exposure (75%).

The k_{UV_{254}/H_2O_2} for the elimination of gene transforming activity was $(5.1 \pm 0.2) \times 10^{-2}$ cm^2/mJ, which was larger than the $k_{UV_{254}}$ by a factor of only 1.1 ($k_{UV_{254}/H_2O_2}/k_{UV_{254}} = 1.1$, Table S1). Thus, even though the $^{\bullet}OH$ exposure significantly accelerated gene degradation (by a factor of 4), its contribution to the elimination of gene transforming activity was not as efficient as expected.

Fig. 6 summarizes the results from this study and the literature on the effect of $^{\bullet}OH$ exposure on degradation of the 851 bp amp^R segment and loss of gene transforming activity (measured using *E. coli* DH5α as recipient strain). Plasmid pUC4k or pUC19 carrying amp^R was treated with UV/H_2O_2 at different conditions of UV wavelength and initial H_2O_2 concentrations, i.e., UV_{254}/H_2O_2 (0.3 mM or 0.5 mM) and $UV_{>290}/H_2O_2$ (10 mM). The $^{\bullet}OH$-induced degradation and deactivation were calculated by subtracting the effect of UV_{254} direct photolysis from the overall results of corresponding UV_{254}/H_2O_2 treatment. Although the statistical analysis showed a significant variation ($p = 0.0149$) in the slopes of linear curves in Fig. 6a, the $k_{^{\bullet}OH,851\ bp}$ values during UV_{254}/H_2O_2 treatment differed only by factors of 0.8–1.5 from that during the $^{\bullet}OH$ only process ($UV_{>290}/H_2O_2$). This suggested that UV_{254}-induced gene damage on the plasmid (e.g., CPDs and pyrimidine adducts) did not have a significant impact on the reactivity of $^{\bullet}OH$ with nucleobase and sugar moieties during UV_{254}/H_2O_2. However, the elimination of gene transforming activity (measured using *E. coli* DH5α as recipient strain) varied significantly in the different treatments. The loss of gene transforming activity attributable to $^{\bullet}OH$ was ~5 times lower in UV_{254}/H_2O_2 processes (UV_{254} and $^{\bullet}OH$ co-exist) as compared to that in $UV_{>290}/H_2O_2$ ($^{\bullet}OH$ only). This indicates that the elimination of gene transforming activity caused by UV_{254} direct photolysis and $^{\bullet}OH$ oxidation were not additive during UV_{254}/H_2O_2. One possible explanation could be that some DNA damage repair pathways such as nucleotide excision repair by *uvr*ABC also repaired $^{\bullet}OH$-induced lesions (e.g., base oxidation) located near the UV-induced lesions, leading to much less extensive loss of transforming activity than would be expected from simple summation of the losses in transforming activity observed for UV_{254} and $^{\bullet}OH$ exposure separately.

The degradation rates of amp^R amplicons (1.0×10^{-1}–3.2×10^{-1} cm^2/mJ) during $UV_{254}/S_2O_8^{2-}$ were also ~4-fold larger than those obtained during UV_{254} (Table S1). $SO_4^{\bullet-}$ is the primary radical generated during UV_{254} photolysis of $S_2O_8^{2-}$. However, $SO_4^{\bullet-}$ can further react with H_2O, OH^-, and Cl^- (sometimes present as an impurity) in aqueous solution to produce $^{\bullet}OH$ (Lutze et al., 2015). Using the degradation kinetics of radical probe compounds (nitrobenzene and *p*CBA) (Figs. S8 and S9), the steady-state concentration of $^{\bullet}OH$ during $UV_{254}/S_2O_8^{2-}$ was determined to be 6.4×10^{-13} M, which was approximately two orders of magnitude smaller than that of $SO_4^{\bullet-}$ (1.8×10^{-11} M) under experimental conditions used here (Text S3). This was consistent with the theoretically estimated values considering all the possible reactions related to $^{\bullet}OH$ formation in the $UV_{254}/S_2O_8^{2-}$ system (Text S4). Despite the much lower concentration, the contribution of $^{\bullet}OH$ to the overall gene damage cannot be ignored, as the amp^R segments appeared to be much more reactive to $^{\bullet}OH$ than $SO_4^{\bullet-}$ (see discussions below). Thus, the percentages of gene degradation attributable to UV_{254} direct photolysis, $SO_4^{\bullet-}$, and $^{\bullet}OH$ during $UV_{254}/S_2O_8^{2-}$ treatment could be estimated as ~23%, ~33%, and ~44%, respectively, where the relative contributions of each pathway to the overall gene damage were calculated based on the observed rate constants for degradation of amp^R amplicons during UV_{254} and $UV_{254}/S_2O_8^{2-}$treatments, the steady-state concentrations of $^{\bullet}OH$ and $SO_4^{\bullet-}$ in $UV_{254}/S_2O_8^{2-}$ experiments, and the second-order rate constants for reactions of $^{\bullet}OH$ and $SO_4^{\bullet-}$ with the amp^R amplicons (Text S5).

The second-order rate constants of $SO_4^{\bullet-}$ with amp^R segments were determined to be in the range of $(1.07–1.96) \times 10^9$ M^{-1} s^{-1}

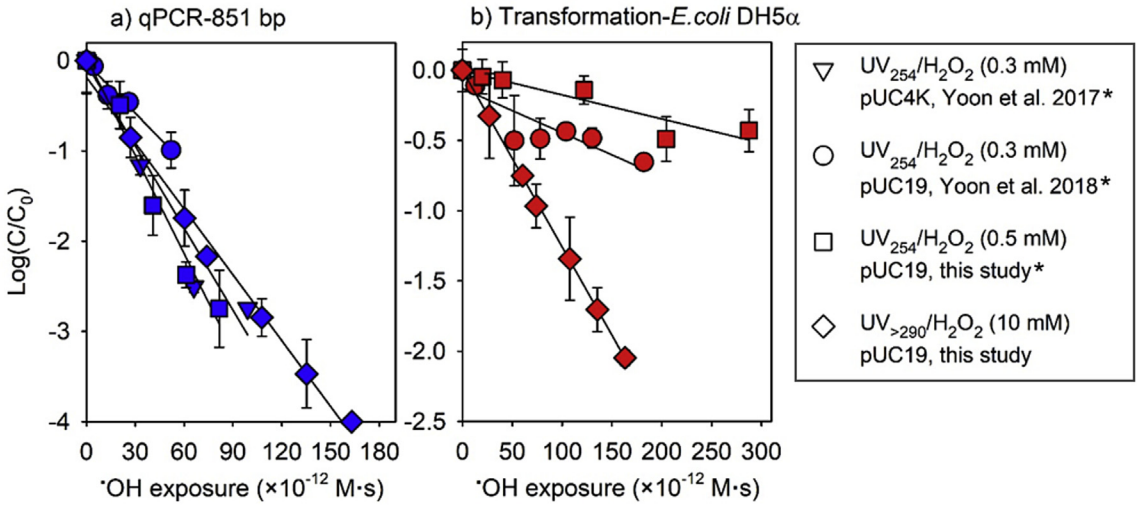

Fig. 6. (a) Degradation of amp^R segment (851 bp) and (b) elimination of gene transforming activity (*E. coli* DH5α as recipient cells) as a function of •OH exposure during UV/H_2O_2 treatments at different UV (254 nm and >290 nm) and H_2O_2 (0.3 mM, 0.5 mM, and 10 mM) conditions. The gene transforming activity was not measured in the study of Yoon et al., (2017) for treating pUC4k with UV_{254}/H_2O_2 (0.3 mM). The values for the data sets designated by (*) represent contributions from •OH exposure only (estimated by subtracting UV_{254} contributions from overall measurements of qPCR signal or transforming activity loss). Error bars represent the standard deviations of triplicate experiments. Lines represent the linear regressions of experimental data.

(Text S5 and Table S2), which were about an order of magnitude lower than the •OH rate constants (Table 1). $SO_4^{\bullet-}$ preferentially adds to the electron-rich sites of the nucleobases (e.g., C_5 of pyrimidines) to generate radical adducts, which decay to nucleobase radicals as intermediates, followed by hydroxylation and oxidation in aqueous solution (von Sonntag, 2006). However, $SO_4^{\bullet-}$ is larger than •OH and negatively charged. Therefore, steric hindrance and electrostatic repulsion might decrease the reactivity of $SO_4^{\bullet-}$ toward negatively charged DNA molecules in comparison to •OH.

Similar to UV_{254}/H_2O_2 processes, the elimination rate of pUC19 transforming activity during $UV_{254}/S_2O_8^{2-}$ treatment was also only slightly larger than that in UV_{254} direct photolysis ($k_{UV_{254}/S_2O_8^{2-}}/k_{UV_{254}} = 1.1$, Table S1), even while the observed amplicon *degradation* rates were ~4-fold faster for $UV_{254}/S_2O_8^{2-}$ compared to UV_{254} direct photolysis. This further supports the above findings that co-exposure to UV_{254} and radicals during UV_{254}-AOPs did not lead to faster transforming activity loss than the separate exposures to UV_{254} and radicals, due to the facile repair of UV_{254} and/or radical-induced DNA damage in host cells.

3.4. Effect of wastewater effluent organic matter on the degradation of amp^R during UV_{254}-AOPs

The efficiencies of amp^R degradation during UV_{254}, UV_{254}/H_2O_2, and $UV_{254}/S_2O_8^{2-}$ experiments were investigated in the presence of EfOM (5.4 mg C/L). The UV 254 nm absorbance of EfOM solution (a_{254}) was 0.1 cm^{-1}. The path length in the petri dish (L) was 1.6 cm. Thus, the water factor, $WF=(1-10^{-a254\cdot L})/(a_{254}\cdot L\cdot \ln 10)$ (Bolton and Linden, 2003), was calculated to be 0.84. The average UV intensity in the solution containing EfOM was then corrected from 0.30 mW/cm^2 to 0.25 mW/cm^2 using the calculated water factor (Lee et al., 2016). The amp^R segments were gradually degraded with increasing UV fluence following first-order kinetics (Fig. 7). Interestingly, the $k_{UV,Amp}$ of each segment during UV_{254} irradiation in the presence of EfOM was approximately 1.2 times higher than the corresponding conditions without EfOM ($p < 0.0001$) (Table S1). Chromophoric dissolved organic matter (DOM) is known to generate reactive species upon UV irradiation, such as triplet excited states of DOM (^{3}DOM*), singlet oxygen, and •OH, which have been proven to contribute to the oxidation of organic pollutants (Chin et al., 2004; Lester et al., 2013; Batista et al., 2016; Rosario-Ortiz and Canonica, 2016). Bacteriophage MS2 was found to be inactivated by ^{3}DOM* and singlet oxygen generated from sunlight irradiation of wastewater and river water DOM isolates (Kohn et al., 2007; Kohn and Nelson, 2007; Rosado-Lausell et al., 2013). The reactive oxygen species (e.g., singlet oxygen, superoxide, H_2O_2) generated during photooxidations involving ^{3}DOM* were proposed to inactivate bacteria by damaging DNA, proteins, and cell membranes (Song et al., 2016; Nelson et al., 2018). Our findings suggest that through its photosensitizing properties, DOM can indirectly contribute to the photodegradation of e-ARGs. Similar results were reported recently on the enhanced photodegradation of pBR322 plasmid-encoded *tet A* and bla_{TEM-1} genes in DOM solution (Zhang et al., 2019b). This degradation pathway might play an especially important role during solar disinfection processes, due to the low UV absorbance characteristics of DNA at high wavelengths (and consequent minimal direct UV photolysis under such conditions).

In contrast, EfOM mainly acted as a radical scavenger during UV_{254}/H_2O_2 and $UV_{254}/S_2O_8^{2-}$ experiments. The k_{UV_{254}/H_2O_2} and $k_{UV_{254}/S_2O_8^{2-}}$ treatment of amp^R segments in the presence of EfOM were each decreased by a factor of ~3 compared to the conditions without EfOM (Table S1). The degradation kinetics of *p*CBA and nitrobenzene (Fig. S10) also confirmed the much lower levels of radicals in the presence of EfOM (e.g., $[SO_4^{\bullet-}]_{ss}$: 9.5×10^{-13} M with EfOM *vs.* 1.8×10^{-11} M without EfOM). Overall, the degradation efficiency of amp^R in the presence of EfOM increased only marginally (within a factor of 1.4) during UV_{254}/H_2O_2 and $UV_{254}/S_2O_8^{2-}$, compared to UV_{254} alone, due to the significant scavenging of radicals by EfOM.

4. Conclusions

- The degradation of amp^R segments and the loss of gene transforming activity followed first-order kinetics with respect to UV fluence and •OH exposure during UV_{254} direct photolysis and •OH oxidation ($UV_{>290}/H_2O_2$). The degradation rate constants of amp^R segments increased with amplicon size, which

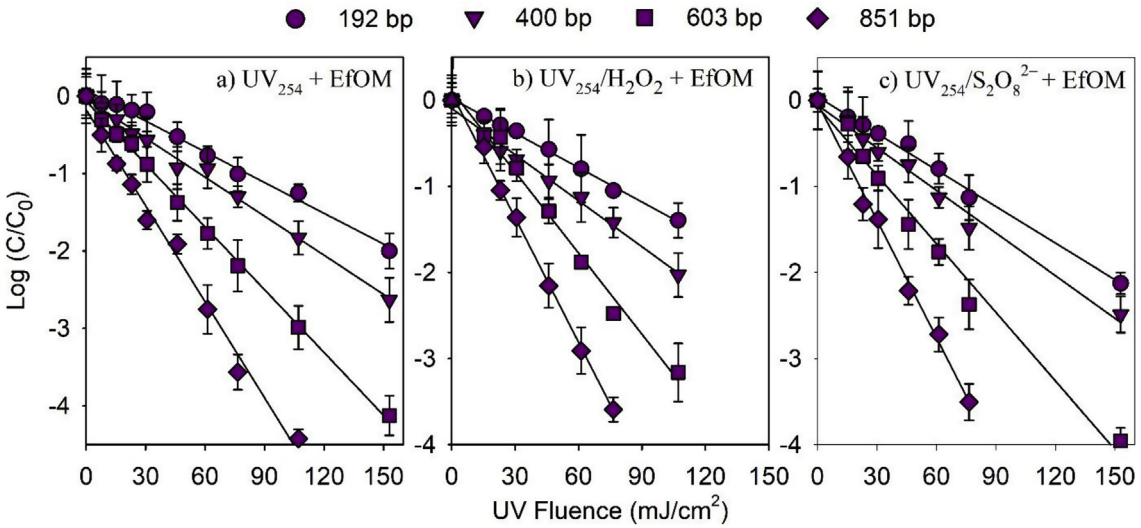

Fig. 7. Degradation of *amp*^{R} segments in the presence of wastewater effluent organic matter (5.4 mg C/L) during the treatment of pUC19 (0.31 μg/mL) with (a) UV_{254}, (b) UV_{254}/H_2O_2 (0.5 mM), and (c) $UV_{254}/S_2O_8^{2-}$ (0.5 mM) at pH 7 (2 mM phosphate buffer). *p*CBA (1 μM) was added in UV_{254}/H_2O_2 experiments for the quantification of •OH, and both *p*CBA and nitrobenzene (each 1 μM) were added in $UV/S_2O_8^{2-}$ experiments for the quantification of •OH and $SO_4^{\bullet-}$. Error bars represent the standard deviations of triplicate experiments. Lines represent the linear regressions of experimental data.

corresponded to the increase in nucleotide bps (and hence, reaction sites) with increased amplicon length. Gel electrophoresis results indicated that UV_{254} (0–130 mJ/cm^2) did not change the supercoiled conformation of pUC19 plasmid, whereas •OH exposure ($0–2.7 \times 10^{-10}$ M•s) led to strand-breaks.

- The loss of gene transforming activity varied depending on the type of recipient cells. Double mutant AB2480, which was deficient in repair genes *uvrA* and *recA*, was the most sensitive to DNA damage induced by UV_{254} direct photolysis and •OH oxidation. The predicted degradation rates for the entire pUC19 plasmid overestimated the loss in transforming activity of pUC19 for all recipient cells other than AB2480, apparently due to the repair of DNA damage by repair-proficient strains.
- The second-order rate constants of •OH with *amp*^{R} segments were determined to be in the range of $8.1 \times 10^9 - 5.6 \times 10^{10}$ ($M^{-1}\ s^{-1}$) and showed a strong linear relationship with the base pair number of *amp*^{R} segments, suggesting that •OH reacts with all nucleobases of plasmid DNA non-selectively. The rate constants of $SO_4^{\bullet-}$ with *amp*^{R} segments were an order of magnitude lower than the corresponding •OH rate constants; thus, the contribution of the trace amount of •OH to the overall gene damage cannot be ignored during $UV_{254}/S_2O_8^{2-}$ treatment.
- Although •OH and $SO_4^{\bullet-}$ significantly accelerated (~75%) the degradation of *amp*^{R} amplicons measured by qPCR during UV_{254}/H_2O_2 and $UV_{254}/S_2O_8^{2-}$ experiments, this only marginally increased the gene deactivation rate (~11%), as gene damage caused by UV_{254} and radical co-exposure appeared to be repaired more efficiently by recipient cells than the gene damage from the separate UV_{254} and radical exposures. Thus, the elimination efficiency of the ARGs' transforming activities was similar for UV_{254} vs UV_{254}-AOPs at the same UV fluence, and the extent of elimination was mainly determined by the level of UV fluence. Because the transforming activity of the *amp*^{R} gene could be lowered by only ~1-log at a typical UV disinfection fluence for water treatment (e.g., 40 mJ/cm^2) but increased to more than 4-logs at an elevated UV fluence for UV-AOPs (e.g., 500 mJ/cm^2), the use of UV-AOPs may still prove beneficial for ARG degradation and deactivation, with the accompanying benefit of improved degradation of trace organic contaminants.
- Reactive species formed from the excitation of chromophoric organic matter appear to contribute to accelerated degradation of *amp*^{R} during UV_{254} irradiation in the presence of EfOM (compared to direct photolysis by UV_{254} alone), whereas EfOM mainly acted as a radical scavenger in UV_{254}/H_2O_2 and $UV_{254}/S_2O_8^{2-}$ experiments.

Declaration of competing interest

The authors declare that they have no known competing financial interests or personal relationships that could have appeared to influence the work reported in this paper.

Acknowledgements

This study was supported by the National Research Foundation funded by the Ministry of Science, ICT and Future Planning (NRF-2020R1A2C2011951). Curtin University (Curtin International Postgraduate Research Scholarship) and Water Research Australia (WaterRA Postgraduate Scholarship) are gratefully acknowledged for providing financial support for M. Nihemaiti. Additional support for H. He and M. C. Dodd from U.S. National Science Foundation Grant Number CBET-1254929 is gratefully acknowledged.

Appendix A. Supplementary data

Supplementary data to this article can be found online at https://doi.org/10.1016/j.watres.2020.115921.

References

Alberts, B., et al., 2002. Molecular Biology of the Cell, fourth ed. Garland Science, New York.
Batista, A.P.S., et al., 2016. Correlating the chemical and spectroscopic characteristics of natural organic matter with the photodegradation of sulfamerazine. Water Res. 93, 20–29.
Bioneer, 2016. AccuPrep® nano-plus plasmid mini/midi/maxi extraction kit. User's Guide Available at: http://us.bioneer.com/Protocol/AccuPrep%20Nano-Plus%20Plasmid%20Extraction%20Kit.pdf.
Bolton, J.R., Linden, K.G., 2003. Standardization of methods for fluence (UV Dose) determination in bench-scale UV experiments. J. Environ. Eng. 129 (3), 209–215.
Buxton, G.V., et al., 1988. Critical Review of rate constants for reactions of hydrated

electrons, hydrogen atoms and hydroxyl radicals (•OH/•O−) in Aqueous Solution. J. Phys. Chem. Ref. Data 17 (2), 513−886.
Cacace, D., et al., 2019. Antibiotic resistance genes in treated wastewater and in the receiving water bodies: a pan-European survey of urban settings. Water Res. 162, 320−330.
Cadet, J., et al., 1999. Hydroxyl radicals and DNA base damage. Mutat. Res. Fund Mol. Mech. Mutagen 424 (1), 9−21.
Cadet, J., Douki, T., 2018. Formation of UV-induced DNA damage contributing to skin cancer development. Photochem. Photobiol. Sci. 17 (12), 1816−1841.
Chang, P.H., et al., 2017. Degradation of extracellular antibiotic resistance genes with UV254 treatment. Environ. Sci. Technol. 51 (11), 6185−6192.
Chin, Y.-P., et al., 2004. Photosensitized degradation of bisphenol A by dissolved organic matter. Environ. Sci. Technol. 38 (22), 5888−5894.
Christou, A., et al., 2017. The potential implications of reclaimed wastewater reuse for irrigation on the agricultural environment: the knowns and unknowns of the fate of antibiotics and antibiotic resistant bacteria and resistance genes − a review. Water Res. 123, 448−467.
Davies, J., Davies, D., 2010. Origins and evolution of antibiotic resistance." microbiology and molecular biology reviews. MMBR (Microbiol. Mol. Biol. Rev.) 74 (3), 417−433.
Dizdaroglu, M., Jaruga, P., 2012. Mechanisms of free radical-induced damage to DNA. Free Radic. Res. 46 (4), 382−419.
Dodd, M.C., 2012. Potential impacts of disinfection processes on elimination and deactivation of antibiotic resistance genes during water and wastewater treatment. J. Environ. Monit. 14 (7), 1754−1771.
Elovitz, M.S., von Gunten, U., 1999. Hydroxyl radical/ozone ratios during ozonation processes. I. The rct concept. Ozone: Sci. Eng. 21 (3), 239−260.
Ferro, G., et al., 2016. Antibiotic resistance spread potential in urban wastewater effluents disinfected by UV/H2O2 process. Sci. Total Environ. 560−561, 29−35.
Ferro, G., et al., 2017. β-lactams resistance gene quantification in an antibiotic resistant Escherichia coli water suspension treated by advanced oxidation with UV/H2O2. J. Hazard Mater. 323, 426−433.
Giannakis, S., et al., 2018. Solar photo-Fenton disinfection of 11 antibiotic-resistant bacteria (ARB) and elimination of representative AR genes. Evidence that antibiotic resistance does not imply resistance to oxidative treatment. Water Res. 143, 334−345.
Görner, H., 1994. New trends in photobiology: photochemistry of DNA and related biomolecules: quantum yields and consequences of photoionization. J. Photochem. Photobiol. B Biol. 26 (2), 117−139.
Guo, M.-T., et al., 2015. Distinguishing effects of ultraviolet exposure and chlorination on the horizontal transfer of antibiotic resistance genes in municipal wastewater. Environ. Sci. Technol. 49 (9), 5771−5778.
He, H., et al., 2019. Degradation and deactivation of bacterial antibiotic resistance genes during exposure to free chlorine, monochloramine, chlorine dioxide, ozone, ultraviolet light, and hydroxyl radical. Environ. Sci. Technol. 53 (4), 2013−2026.
Hiller, C.X., et al., 2019. Antibiotic microbial resistance (AMR) removal efficiencies by conventional and advanced wastewater treatment processes: a review. Sci. Total Environ. 685, 596−608.
Hong, P.-Y., et al., 2018. Reusing treated wastewater: consideration of the safety aspects associated with antibiotic-resistant bacteria and antibiotic resistance genes. Water 10 (3).
Kisker, C., et al., 2013. Prokaryotic Nucleotide Excision Repair 5 (3) a012591−a012591.
Kohn, T., et al., 2007. Association with natural organic matter enhances the sunlight-mediated inactivation of MS2 coliphage by singlet oxygen. Environ. Sci. Technol. 41 (13), 4626−4632.
Kohn, T., Nelson, K.L., 2007. Sunlight-mediated inactivation of MS2 coliphage via exogenous singlet oxygen produced by sensitizers in natural waters. Environ. Sci. Technol. 41 (1), 192−197.
Lee, Y., et al., 2016. Organic contaminant abatement in reclaimed water by UV/H2O2 and a combined process consisting of O3/H2O2 followed by UV/H2O2: prediction of abatement efficiency, energy consumption, and byproduct formation. Environ. Sci. Technol. 50 (7), 3809−3819.
Lester, Y., et al., 2013. Production of photo-oxidants by dissolved organic matter during UV water treatment. Environ. Sci. Technol. 47 (20), 11726−11733.
Liu, S.-S., et al., 2018. Chlorine disinfection increases both intracellular and extracellular antibiotic resistance genes in a full-scale wastewater treatment plant. Water Res. 136, 131−136.
Lorenz, M.G., Wackernagel, W., 1994. Bacterial gene transfer by natural genetic transformation in the environment. Microbiol. Rev. 58 (3), 563−602.
Luby, E., et al., 2016. Molecular methods for assessment of antibiotic resistance in agricultural ecosystems: prospects and challenges. J. Environ. Qual. 45 (2), 441.
Lutze, H.V., et al., 2015. Sulfate radical-based water treatment in presence of chloride: formation of chlorate, inter-conversion of sulfate radicals into hydroxyl radicals and influence of bicarbonate. Water Res. 72, 349−360.
Mao, D., et al., 2014. Persistence of extracellular DNA in river sediment facilitates antibiotic resistance gene propagation. Environ. Sci. Technol. 48 (1), 71−78.
McKinney, C.W., Pruden, A., 2012. Ultraviolet disinfection of antibiotic resistant bacteria and their antibiotic resistance genes in water and wastewater. Environ. Sci. Technol. 46 (24), 13393−13400.
Michael-Kordatou, I., et al., 2015. Erythromycin oxidation and ERY-resistant Escherichia coli inactivation in urban wastewater by sulfate radical-based oxidation process under UV-C irradiation. Water Res. 85, 346−358.
Nagler, M., et al., 2018. Extracellular DNA in natural environments: features, relevance and applications. Appl. Microbiol. Biotechnol. 102 (15), 6343−6356.
Nelson, K.L., et al., 2018. Sunlight-mediated inactivation of health-relevant microorganisms in water: a review of mechanisms and modeling approaches. Environ. Sci.: Process. Impacts 20 (8), 1089−1122.
Neta, P., et al., 1977. Rate constants and mechanism of reaction of SO4·- with aromatic compounds. J. Am. Chem. Soc. 99 (1), 163−164.
Neta, P., et al., 1988. Rate constants for reactions of inorganic radicals in aqueous solution. J. Phys. Chem. Ref. Data 17 (3), 1027−1284.
Osińska, A., et al., 2020. Small-scale wastewater treatment plants as a source of the dissemination of antibiotic resistance genes in the aquatic environment. J. Hazard Mater. 381, 121221.
Pruden, A., 2014. Balancing water sustainability and public health goals in the face of growing concerns about antibiotic resistance. Environ. Sci. Technol. 48 (1), 5−14.
Rosado-Lausell, S.L., et al., 2013. Roles of singlet oxygen and triplet excited state of dissolved organic matter formed by different organic matters in bacteriophage MS2 inactivation. Water Res. 47 (14), 4869−4879.
Rosario-Ortiz, F.L., Canonica, S., 2016. Probe compounds to assess the photochemical activity of dissolved organic matter. Environ. Sci. Technol. 50 (23), 12532−12547.
Shanehbandi, D., et al., 2013. Vibration and glycerol-mediated plasmid DNA transformation for Escherichia coli. FEMS (Fed. Eur. Microbiol. Soc.) Microbiol. Lett. 348 (1), 74−78.
Shinohara, A., Ogawa, T., 1995. Homologous recombination and the roles of double-strand breaks. Trends Biochem. Sci. 20 (10), 387−391.
Shou, W., et al., 2019. Substituted aromatic-facilitated dissemination of mobile antibiotic resistance genes via an antihydrolysis mechanism across an extracellular polymeric substance permeable barrier. Environ. Sci. Technol. 53 (2), 604−613.
Sinha, R.P., Häder, D.-P., 2002. UV-induced DNA damage and repair: a review. Photochem. Photobiol. Sci. 1 (4), 225−236.
Smith, K.C., Wang, T.-C.V., 1989. recA-dependent DNA repair processes. Bioessays 10 (1), 12−16.
Song, K., et al., 2016. Application of ultraviolet light-emitting diodes (UV-LEDs) for water disinfection: a review. Water Res. 94, 341−349.
Stefan, M.I., 2018. Advanced Oxidation Processes for Water Treatment. Fundamentals and Applications. IWA Publishing.
Teebor, G.W., et al., 1988. The repairability of oxidative free radical mediated damage to DNA: a review. Int. J. Radiat. Biol. 54 (2), 131−150.
Vikesland, P.J., et al., 2017. Toward a comprehensive strategy to mitigate dissemination of environmental sources of antibiotic resistance. Environ. Sci. Technol. 51 (22), 13061−13069.
von Sonntag, C., 2006. Free-radical-induced DNA Damage and its Repair: A Chemical Perspective. Springer, Heidelberg, Berlin.
Wu, D., et al., 2019. Urban and agriculturally influenced water contribute differently to the spread of antibiotic resistance genes in a mega-city river network. Water Res. 158, 11−21.
Yoon, Y., et al., 2017. Inactivation efficiency of plasmid-encoded antibiotic resistance genes during water treatment with chlorine, UV, and UV/H2O2. Water Res. 123, 783−793.
Yoon, Y., et al., 2018. Elimination of transforming activity and gene degradation during UV and UV/H2O2 treatment of plasmid-encoded antibiotic resistance genes. Environ. Sci.: Water Res. Technol. 4 (9), 1239−1251.
Zhang, Y., et al., 2017. "Subinhibitory concentrations of disinfectants promote the horizontal transfer of multidrug resistance genes within and across genera.". Environ. Sci. Technol. 51 (1), 570−580.
Zhang, Y., et al., 2018. Cell-free DNA: a neglected source for antibiotic resistance genes spreading from WWTPs. Environ. Sci. Technol. 52 (1), 248−257.
Zhang, T., et al., 2019a. Removal of antibiotic resistance genes and control of horizontal transfer risk by UV, chlorination and UV/chlorination treatments of drinking water. Chem. Eng. J. 358, 589−597.
Zhang, X., et al., 2019b. Enhanced photodegradation of extracellular antibiotic resistance genes by dissolved organic matter photosensitization. Environ. Sci. Technol. 53 (18), 10732−10740.
Zheng, X., et al., 2014. Contribution of effluent organic matter (EfOM) to ultrafiltration (UF) membrane fouling: isolation, characterization, and fouling effect of EfOM fractions. Water Res. 65, 414−424.
Zheng, J., et al., 2017. Effects and mechanisms of ultraviolet, chlorination, and ozone disinfection on antibiotic resistance genes in secondary effluents of municipal wastewater treatment plants. Chem. Eng. J. 317, 309−316.